



Laser-cavity locking utilizing beam ellipticity: accessing the 10^{-7} instability scale relative to cavity linewidth

FRITZ DIORICO,  ARTEM ZHUTOV, AND ONUR HOSTEN*

Institute of Science and Technology Austria, Klosterneuburg, Austria

**onur.hosten@ist.ac.at*

Received 4 October 2023; revised 4 December 2023; accepted 10 December 2023; published 3 January 2024

Frequency-stable lasers form the back bone of precision measurements in science and technology. Such lasers typically attain their stability through frequency locking to reference cavities. State-of-the-art locking performances to date had been achieved using frequency modulation based methods, complemented with active drift cancellation systems. We demonstrate an all passive, modulation-free laser-cavity locking technique (squash locking) that utilizes changes in spatial beam ellipticity for error signal generation, and a coherent polarization post-selection for noise resilience. By comparing two identically built proof-of-principle systems, we show a frequency locking instability of 5×10^{-7} relative to the cavity linewidth at 10 s averaging. The results surpass the demonstrated performances of methods engineered over the last five decades, potentially enabling an advancement in the precision control of lasers, while creating avenues for bridging the performance gaps between industrial grade lasers with scientific ones due to the afforded simplicity and scalability. © 2024 Optica Publishing Group under the terms of the [Optica Open Access Publishing Agreement](#)

<https://doi.org/10.1364/OPTICA.507451>

1. INTRODUCTION

Laser frequency stabilization is indispensable in the science and engineering of atomic time keeping [1], gravitational wave detection [2], tests of relativity [3], atom interferometry [4], and in the quantum control of various systems such as atoms [5], nanoparticles [6], and mechanical oscillators [7]—to name a few. As an example, contemporary atomic clocks require milliHertz-linewidth lasers to probe long-lived optical atomic transitions, and the level of precision in stabilization of laser frequencies to reference optical cavities plays a crucial role in reaching the state-of-the-art performance levels [8,9]. On the other hand, there has been a growing interest in scientific grade lasers that are compact and field-deployable for industry applications [10,11]. Such high-performance lasers typically operate on the principle of self-injection locking, and further utilize reference optical cavities [11]. Achieving a large mode-hop-free tuning range while maintaining spectrally low-noise operation in these systems requires multiple instances of relative frequency monitoring and stabilization [12–14], favoring simple and scalable techniques. A number of methods have been developed over the decades to address the task of locking lasers to cavities. These include: side-of-fringe intensity methods [15], polarization based methods [16–18], frequency modulation techniques including transmission modulation [19,20] and the Pound–Drever–Hall (PDH) reflection method [21], and lastly, spatial mode interference methods [22–25].

Preference for a specific method could be application dependent, but due to its stability and versatility, the PDH technique—utilizing radio-frequency modulation/demodulation

of an optical carrier—has become a general standard. Achieving the most demanding locking stabilities of one part in 10^5 – 10^6 of a cavity linewidth has further required additional layers of active feedback mechanisms to reduce the residual amplitude (RAM) modulation [26], which typically limits the lock point stability of a PDH setup. A purely passive and reduced-complexity method that could compete with these highly engineered setups could be beneficial for all applications, especially when electro- and acousto-optic devices used for modulation are particularly undesirable [27,28]. The simplicity and scalability of such a method for laser-cavity locking is also paramount to bridging the gap between scientific and industrial laser standards.

Here we develop a precision laser frequency stabilization scheme that utilizes completely passive optical elements. The main method consists of monitoring the change in the spatial ellipticity of a beam reflected from a cavity. This method is further enhanced with a pre- and a post-selection of the beam polarization to coherently suppress technical noise that limits system performance. Notably, through this enhancement technique, we also uncover a curious physical phenomenon where the post-selection gives rise to an effective cavity with variable loss or gain.

Our scheme differs from previous spatial mode methods in its robustness of implementation and insensitivity to alignment drifts. Further, it differs from previous polarization based methods in its utilization of polarization only to reject noise. These aspects enable us to realize the true potential of modulation-free schemes. Both aspects of the scheme are cavity geometry independent, applicable

to linear or ring cavities (see Supplement 1), and can be used independently of each other. To hint at the versatility of this developed method, we note that it is already spinning a separate application that could fill a void in laser industry: high-quality monitoring and stabilization of laser diode injection locking [29–31].

2. CONCEPTS

To understand the main stabilization method, one needs to recall the Hermite–Gaussian (HG) spatial modes supported by an optical cavity [32]. Here, of interest are the fundamental HG mode labeled “00” and a specific second-order mode that we label “+” (due to its visual appearance—Fig. 1(a), which is a superposition of the more familiar “02” and “20” HG modes (see Supplement 1). A slightly elliptical beam with a horizontal/vertical orientation can mathematically be decomposed into a main “00” component and a small “+” component [Fig. 1(b)]. For such a beam, the phase difference between these two components encodes the information about ellipticity. When incident on the cavity near a “00” resonance, only the “00” component builds up inside the cavity, acquiring a phase shift in the process, and giving rise to a change in the relative phase between the two components outside of the cavity. Through this mode-dependent phase shift, the reflected beam can be made to acquire opposite ellipticities on opposite sides of the resonance [Fig. 1(c)]. From the perspective of cavity design, the only requirement for proper operation is for the “00” mode not to be spectrally degenerate with the second-order modes. To harness this effect we use a quadrant photodiode (QPD), subtracting the sums of the diagonals to obtain an error signal proportional

to the spatial ellipticity of the beam [Figs. 1(b) and 1(c); see also Supplement 1 for QPD electronics].

The detected signal can be thought of as an interference between the resonating “00” mode that leaks out of the cavity, and the second-order “+” mode that promptly reflects from the cavity to form a phase reference. This detection modality is insensitive to alignment drifts and fluctuations, since small misalignments simply generate first-order modes in the mode decomposition [23]. A limitation to stability is still posed, for example, by residual fluctuations in the incident beam shape, attributable to the alteration of second-order mode components—affecting the phase reference. To help alleviate this residual limitation, we utilize the mentioned polarization pre- and post-selection procedure—or simply put, the polarization filtering process.

Intuitively, the polarization filtering allows one to directly perform a differential measurement between the signals that would be generated by two separate polarization components of light incident on the cavity. With polarization-resolved cavity resonances, one polarization component can build up resonantly in the cavity while the other orthogonal polarization component reflects promptly, serving as a reference for the noise originating prior to the cavity. Following polarization filtering, the overall signal comes about through an interference between the amplitudes from the two polarization components. This effective differential measurement implemented by the polarization filtering then isolates the cavity signal. Curiously, this phenomenon affords a simple universal description in the form of an effective loss-tunable cavity. From an application point of view, however, the final filtering setting adapted for this work simply enforces a complete destructive

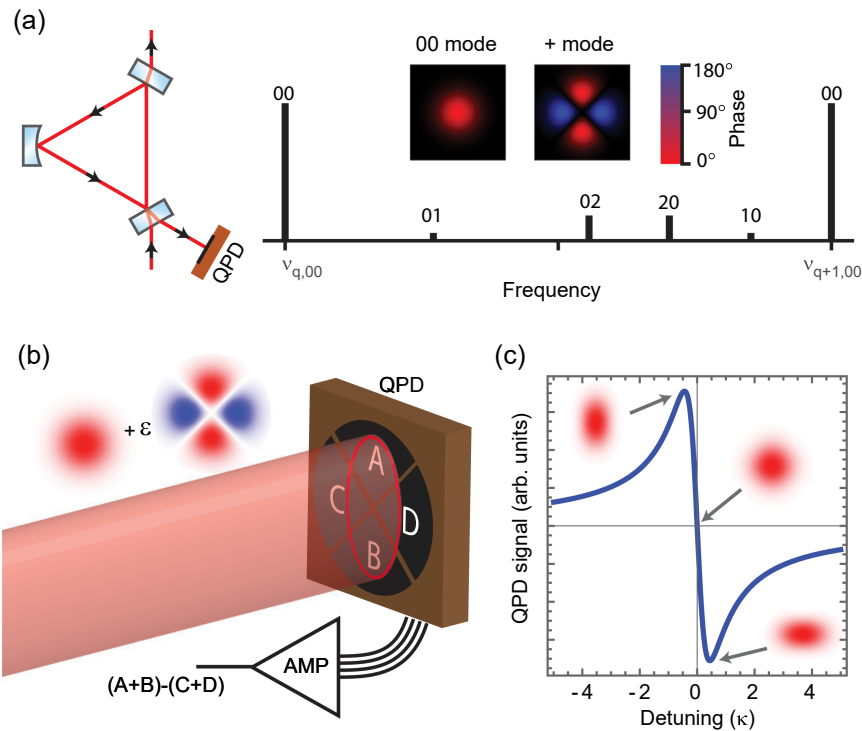


Fig. 1. Conceptual illustration. (a) Geometry of the utilized cavity, and its relevant modes within one free spectral range (mirrors: two plane, one 5-cm radius-of-curvature). Inset: spatial amplitude structure of the “00” and the “+” modes. In terms of the native cavity modes, the “+” mode appears as a superposition of the “02” and “20” modes. Alignment drifts populate the “01” and “10” modes. The unusual spectral ordering of the “10” mode originates from the odd number of mirrors in conjunction with geometric reflection phases. QPD, quadrant photodiode; q , longitudinal mode number; $\nu_{q,00}$, frequency of the q th “00” mode. (b) Beam ellipticity detection using a QPD, and mode decomposition of a slightly elliptical beam. ϵ , a small complex number; AMP, transimpedance amplifier. (c) Laser frequency dependence of the QPD signal near the “00” mode resonance. κ , cavity full-linewidth.

interference between the two amplitudes when the cavity is exactly on resonance.

We describe the polarization filtering effect efficiently using the weak-value concept [33]. This concept has been utilized over the last decade to amplify small signals in optical settings [34–37] with mostly a good understanding of its benefits [38,39]. Nevertheless an understanding of this formalism is not required to follow the rest of the article. We will summarize the result here and utilize the effect as intended—interested readers can find more information in Supplement 1.

In this formalism, with the polarization degree of freedom included, the cavity reflection coefficient is replaced by a reflection operator \hat{r} acting on the input polarization state $|\psi_1\rangle$. When a post-selection onto state $|\psi_2\rangle$ is made, the resulting effective reflection coefficient r_w [Fig. 2(a)] is given by the weak-value of the reflection operator (see Supplement 1):

$$r_w = \frac{\langle\psi_2|\hat{r}|\psi_1\rangle}{\langle\psi_2|\psi_1\rangle} = 1 - \gamma' \frac{1}{1 - i\frac{\delta}{\kappa/2}}. \quad (1)$$

This effective reflection coefficient is of the same form as a reflection coefficient from a regular high-finesse cavity, except with a variable effective loss parameter γ' (at fixed cavity linewidth κ). The imaginary part of this equation gives the mathematical form of the error signal generated by the QPD. Here δ is the laser-cavity frequency detuning, κ is the full-width cavity linewidth, and $\gamma' = A\gamma$. The true loss parameter γ is a dimensionless constant characterizing the roundtrip losses in the cavity, where $\gamma < 1$, $\gamma = 1$, $\gamma > 1$, and $\gamma > 2$ can be identified respectively with the under-coupled, impedance-matched, over-coupled, and cavity-gain regimes. The “amplification” parameter A depends on the specific post-selection, and it is real-valued for linear polarization

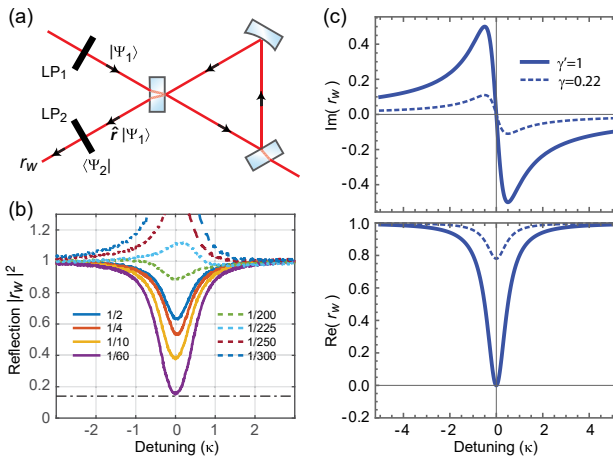


Fig. 2. Weak value enhancement: effective cavity under polarization pre- and post-selection. (a) Input/output polarizers are used to obtain the weak-value r_w of the reflection operator \hat{r} , resulting in an effective cavity with tunable reflection. LP, linear polarizer. (b) Measured normalized reflection power for different post-selection configurations. Curves are labeled by their off-resonant remaining power fraction $|\langle\psi_2|\psi_1\rangle|^2$. 1/2-curve, same as original cavity reflection curve; $\sim 1/60$ -curve, effective impedance matched ($\gamma' = 1$) configuration. Dashed-dotted line: intensity contribution level from the non-“00” mode components. For a discussion on observed asymmetries in the curves, see Supplement 1. (c) Real and imaginary parts of r_w for an input mode matched to the “00” mode (theory), illustrating the advantages of post-selection: effective increase in the slope of the error signal, and minimization of optical power on the QPD near the locking point.

states $|\psi_1\rangle$ and $|\psi_2\rangle$. While it is a function of polarizer angles, operationally it can be related to the remaining power fraction $|\langle\psi_1|\psi_2\rangle| \approx 1/(2A + 1)^2$ after post-selection when the light is off-resonant (see Supplement 1).

3. RESULTS AND DISCUSSION

We first experimentally demonstrate the variability of the effective cavity loss parameter γ' in Fig. 2(b) by observing the post-selection dependence of the reflected power from the cavity. Tuning the post-selection to the effective impedance-matched configuration reduces noise for the purposes of frequency stabilization. In this configuration, the non-signal-generating beam components incident on the QPD are strongly filtered out, while signal generating parts are attenuated less. In other words, although the actual signal magnitude drops, the slope of the normalized error signal increases [Fig. 2(c)], and sensitivity to beam shape or intensity fluctuations reduces. See Supplement 1 for additional details.

To demonstrate the performance of our stabilization scheme itself, we build two identical copies of the locking setup [Fig. 3(a)],

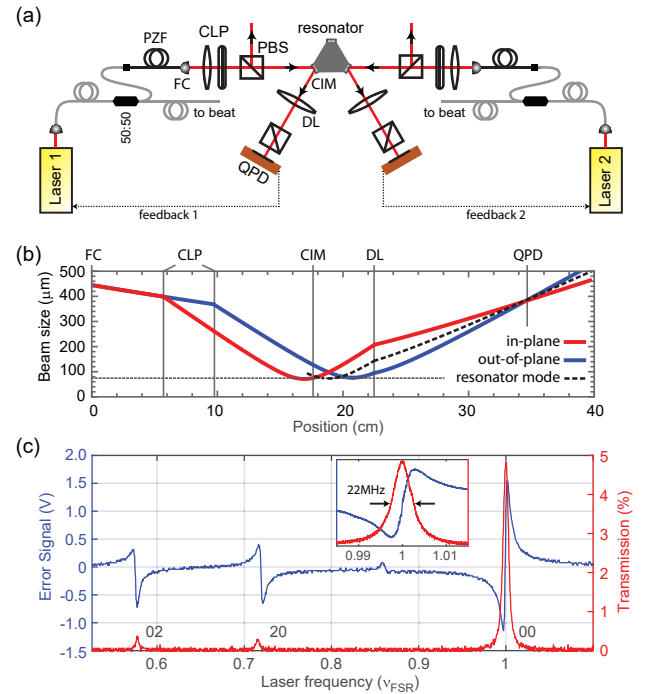


Fig. 3. Experimental setup. (a) Setup for locking two identical lasers to a common optical cavity. At the beatnote setup (not shown), one path is frequency shifted by 80 MHz with an acousto-optic modulator before combining the paths on a beam splitter leading to a fast photodiode. Except the lasers, the setup is enclosed in a metal box for temperature stability and reduced air flow. CLP, cylindrical lens pair, 150-mm convex each, one oriented with axis in-plane the other out-of-plane; FC, fiber collimator with adjustable focus; “50:50,” polarization maintaining fiber splitter; PZF, polarizing fiber; PBS, rotatable polarizing beam splitter; CIM, cavity input mirror; DL, detection lens, 100-mm convex spherical; QPD, quadrant photodiode (Fig. 1b). (b) Location of the relevant elements, and resulting beam properties. Black dotted line: 74- μm mean cavity mode waist (84 μm in-plane, 65 μm out-of-plane). Precise location of DL is not important; DL to QPD distance matters. (c) Typical error signal along with cavity transmission. Inset: zoom-in to the “00” resonance region after fine tuning the positioning of the elements for minimizing asymmetries in the error signal.

and stabilize two separate lasers to two degenerate counter-propagating “00” modes of a triangular ring cavity. Locking two independent lasers to a common cavity has been the standard method of isolating and evaluating the performance of the locking methodology irrespective of cavity properties [20,40,41]. To assess stability, we split-off 50% of the power from the lasers to monitor the beating frequency of the lasers on a fast photodiode using a frequency counter (SRS FS740). Additional details on cavity construction and alignment can be found in Supplement 1.

The implementation of the locking scheme relies on beam shaping for achieving opposite beam ellipticities on opposite sides of the resonance [Fig. 1(c)]. This goal requires the phase difference between the “00” and the “+” components of the beam at the QPD location to be $\pi/2$ radians when the frequency is matched to the “00” resonance. In this configuration the interference of the two components results in a circular beam profile at the QPD, yielding a zero error signal. When the frequency is detuned from resonance, the reflected “00” component acquires an additional phase shift determined by Eq. (1), directly altering the phase difference at the QPD location. For detunings of opposite sign, the phase-shifted interference results in opposite beam ellipticities, yielding opposite sign error signals. Note that the phase shift recedes to its on-resonance value for large detunings, rendering the beam circular once more far off-resonance. This allows us to do alignment and tuning while off-resonance.

The required beam shaping is achieved using a cylindrical lens pair (CLP), through which a circular input beam is astigmatically focused. The distance between the CLP determines the amount of light in the “+” mode, amounting to 10% of the total power (400 μ W) in our demonstration. Lens positions are aligned such that, as the beam propagates it reaches back to a circular profile at the QPD location when the light is off-resonance [Fig. 3(b)]. The size of this circular beam needs to match that of

the forward-propagated cavity “00” mode to maximize the signal. For additional details on the design principle of the CLP and its relation to the error signal size, see Supplement 1.

The cavity utilized in this work has a full-linewidth of 22 MHz and a finesse of 195 for the “00” mode (and a corresponding free spectral range of $\nu_{\text{FSR}} = 4.28$ GHz). Two independent external cavity diode lasers at 780 nm are employed to probe the cavity. Each laser has an intrinsic-linewidth of 500 KHz. A typical error signal from this setup is shown in Fig. 3(c) as one varies the frequency of one of the lasers. For reference, the largest peak of the signal here corresponds to a beam aspect ratio of about 1.3. To independently lock the frequencies of the two lasers to a common resonance, the obtained error signals are fed back to the currents of the respective lasers through feedback controllers (see Supplement 1).

A comparison between different optical frequency stabilization systems can be made by characterizing the performance as a fractional instability with respect to the cavity linewidth. In Fig. 4(a), we present the performance of the implemented scheme while locked to a “00” mode resonance, and compare it to the best known implementations of other stabilization methods. It can be seen that we enter the 10^{-7} locking instability regime for averaging times between 0.25 and 100 s, surpassing previous state-of-the-art, and reaching 5×10^{-7} instability at 10 s averaging. The explicit improvement brought by the post-selection is also illustrated in Fig. 4(b). Note that prior to this work, the tightest demonstrated laser-cavity locking was achieved using the transmission modulation method [20] [Fig. 4(a)].

When extrapolating the results obtained in this work to different applications and cavity parameter ranges, it should be noted that absolute instabilities will scale down together with the cavity linewidth. This is due to the fact that typical sources of problematic instabilities originate from fluctuations in the error signal shape.

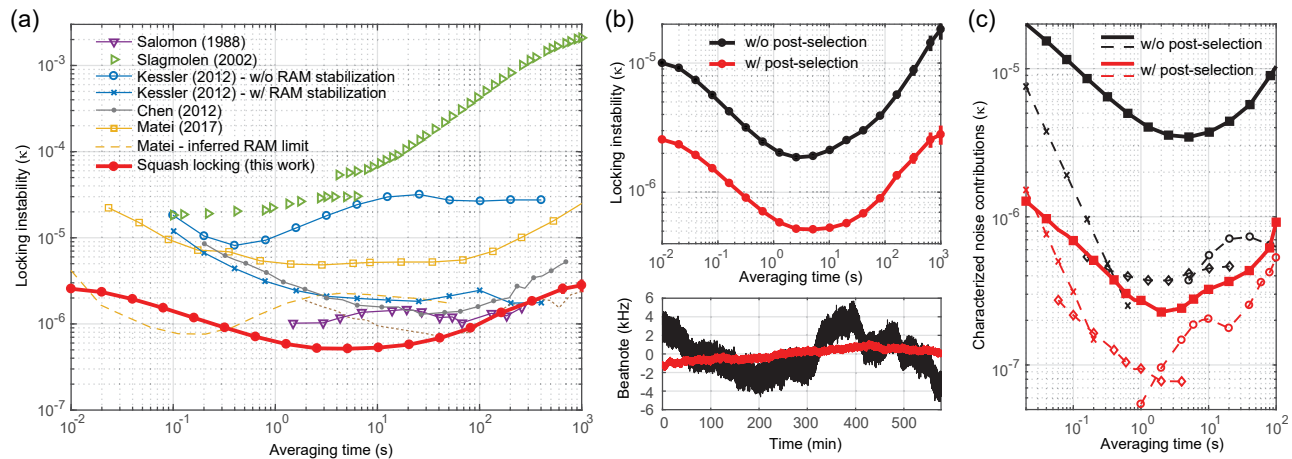


Fig. 4. Laser frequency locking performance. (a) Achieved frequency locking instability for an individual laser relative to cavity linewidth (filled circles). Allan deviation of a 10-h recorded beatnote is taken and equal instabilities for the two locks is assumed. Comparison of locking instability with previous work: Salomon [20]: transmission modulation method; Slagmolen [40]: double-passed “tilt locking” method; Matei [9,42]: PDH method, and its inferred limit due to RAM; Kessler [8]: PDH method out-of-loop noise floor characterization with and without RAM stabilization (arXiv:1112.3854 for these data); Chen [41]: PDH method, all elements inside vacuum. Dotted lines [43]: recent engineering of RAM levels—no demonstration of an actual laser-cavity locking at such levels. Data are extracted and expressed relative to cavity linewidths utilized in each work (see Supplement 1). (b) Top: comparison of achieved instability for operation with (red) and without (black) post-selection; bottom: corresponding beatnote traces. Throughout, error bars indicate ± 1 standard deviation. (c) Estimated limitations to stability for the two cases: “with” post-selection (everything red), and “without” post-selection (everything black). Each case is further split into two: the dominant contribution (solid lines), and the subdominant contributions (dashed lines). The dominant contribution is the input beam shape noise: a comparison with part (b) shows this is the main limitation to the performance. The subdominant contributions are additionally detailed for each case through the utilized symbols: measured in-loop error signal noise (crosses)—prominent at short timescales; QPD dark noise (diamonds)—prominent at intermediate timescales; laser intensity drift noise (circles)—prominent at long timescales (circles).

For example, in the case of absolute optical frequency stabilization to very narrow linewidth cavities [9], the achievable locking performance relative to the cavity linewidth should be preserved. Nevertheless there will clearly be other challenges to the overall task coming from factors that are not related to the locking method, such as keeping the absolute length of the cavity stable.

A characterization of various noise sources [Fig. 4(c); see Supplement 1] reveals that the residual fluctuations of the incident beam shape constitute the dominant limitation to the currently achieved instability level. A major source of this instability is the thermal-stress-induced polarization changes inside the launching fibers, which we observed to directly translate into spatial beam ellipticity fluctuations. In fact, we note that switching from polarization maintaining fibers to polarizing fibers [Fig. 3(a)] had provided nearly an order of magnitude improvement, allowing us to reach the current results. Further stability improvements will require better control over the input beam shape stability. For a discussion of additional effects on achievable performance, such as the long-term temperature drifts or initial laser linewidths, see Supplement 1.

4. CONCLUSION

A generic optical-cavity application can integrate “squash locking” as a plug-and-play method, benefiting from simplicity, robustness, and performance. The lack of RF modulation, which avoids spectral contamination and electromagnetic interference, makes the technique particularly suited for applications like optical frequency conversion [44] or stabilization of laser injection locking [29,45]. For high-performance applications, such as space based laser ranging (including gravitational wave detection) or development of optical frequency standards [9], there are often additional requirements that the technique is capable of delivering: direct compatibility with low-light-level measurements (see Supplement 1), and direct integration compatibility with ultralow-vibration-sensitivity cavities (see Supplement 1). Recently, utilizing the “tilt locking” technique [23], a modulation-free laser locking system for ranging applications was demonstrated [46], showing compatibility with demanding space mission requirements. With the current technique, such systems could be implemented or improved more easily. Lastly, given its direct compatibility with on-chip systems such as dielectric whispering-gallery cavities (see Supplement 1), the technique can benefit industrial optical communication systems requiring narrow linewidth lasers [47], and help put scientific grade laser performances at the disposal of industry due to its simplicity and scalability.

Funding. Institute of Science and Technology Austria.

Acknowledgment. We thank Rishabh Sahu and Sebastian Wald for technical contributions to the experiment.

Disclosures. OH, FD: Institute of Science and Technology Austria (P).

Data availability. Data underlying the results presented in this paper are not publicly available at this time but may be obtained from the authors upon reasonable request.

Supplemental document. See Supplement 1 for supporting content.

REFERENCES

1. B. J. Bloom, T. L. Nicholson, J. R. Williams, *et al.*, “An optical lattice clock with accuracy and stability at the 10^{-18} level,” *Nature* **506**, 71–75 (2014).
2. B. Abbott, R. Abbott, T. D. Abbott, *et al.*, “Observation of gravitational waves from a binary black hole merger,” *Phys. Rev. Lett.* **116**, 061102 (2016).
3. N. Gürlebeck, L. Wörner, T. Schuldt, *et al.*, “Boost: A satellite mission to test lorentz invariance using high-performance optical frequency references,” *Phys. Rev. D* **97**, 124051 (2018).
4. J. Rudolph, T. Wilkason, M. Nantel, *et al.*, “Large momentum transfer clock atom interferometry on the 689 nm intercombination line of strontium,” *Phys. Rev. Lett.* **124**, 083604 (2020).
5. O. Hosten, N. J. Engelsen, R. Krishnakumar, *et al.*, “Measurement noise 100 times lower than the quantum-projection limit using entangled atoms,” *Nature* **529**, 505–508 (2016).
6. S. Kuhn, P. Asenbaum, A. Kosloff, *et al.*, “Cavity-assisted manipulation of freely rotating silicon nanorods in high vacuum,” *Nano Lett.* **15**, 5604–5608 (2015).
7. M. Aspelmeyer, T. J. Kippenberg, and F. Marquardt, “Cavity optomechanics,” *Rev. Mod. Phys.* **86**, 1391–1452 (2014).
8. T. Kessler, C. Hagemann, C. Grebing, *et al.*, “A sub-40-mHz-linewidth laser based on a silicon single-crystal optical cavity,” *Nat. Photonics* **6**, 687–692 (2012).
9. D. G. Matei, T. Legero, S. Häfner, *et al.*, “1.5 μm lasers with sub-10 mHz linewidth,” *Phys. Rev. Lett.* **118**, 263202 (2017).
10. D. J. Blumenthal, H. Ballani, R. O. Behunin, *et al.*, “Frequency-stabilized links for coherent WDM fiber interconnects in the datacenter,” *J. Lightwave Technol.* **38**, 3376–3386 (2020).
11. J. Guo, C. A. McLemore, C. Xiang, *et al.*, “Chip-based laser with 1-Hertz integrated linewidth,” *Sci. Adv.* **8**, eabp9006 (2022).
12. S. I. Ohshima and H. Schnatz, “Optimization of injection current and feedback phase of an optically self-locked laser diode,” *J. Appl. Phys.* **71**, 3114–3117 (1992).
13. J. Labaziewicz, P. Richerme, K. R. Brown, *et al.*, “Compact, filtered diode laser system for precision spectroscopy,” *Opt. Lett.* **32**, 572–574 (2007).
14. K. Hayasaka, “Modulation-free optical locking of an external-cavity diode laser to a filter cavity,” *Opt. Lett.* **36**, 2188–2190 (2011).
15. R. L. Barger, M. Sorem, and J. Hall, “Frequency stabilization of a cw dye laser,” *Appl. Phys. Lett.* **22**, 573–575 (1973).
16. T. Hänsch and B. Couillaud, “Laser frequency stabilization by polarization spectroscopy of a reflecting reference cavity,” *Opt. Commun.* **35**, 441–444 (1980).
17. P. Asenbaum and M. Arndt, “Cavity stabilization using the weak intrinsic birefringence of dielectric mirrors,” *Opt. Lett.* **36**, 3720–3722 (2011).
18. S. Moriwaki, T. Mori, K. Takeno, *et al.*, “Frequency discrimination method making use of polarization selectivity of triangular optical cavity,” *Appl. Phys. Express* **2**, 016501 (2009).
19. A. White, “Frequency stabilization of gas lasers,” *IEEE J. Quantum Electron.* **1**, 349–357 (1965).
20. C. Salomon, D. Hils, and J. L. Hall, “Laser stabilization at the millihertz level,” *J. Opt. Soc. Am. B* **5**, 1576–1587 (1988).
21. R. W. P. Drever, J. L. Hall, F. V. Kowalski, *et al.*, “Laser phase and frequency stabilization using an optical resonator,” *Appl. Phys. B* **31**, 97–105 (1983).
22. C. E. Wieman and S. L. Gilbert, “Laser-frequency stabilization using mode interference from a reflecting reference interferometer,” *Opt. Lett.* **7**, 480–482 (1982).
23. D. A. Shaddock, M. B. Gray, and D. E. McClelland, “Frequency locking a laser to an optical cavity by use of spatial mode interference,” *Opt. Lett.* **24**, 1499–1501 (1999).
24. J. Miller and M. Evans, “Length control of an optical resonator using second-order transverse modes,” *Opt. Lett.* **39**, 2495–2498 (2014).
25. R. Zullo, A. Giorgini, S. Avino, *et al.*, “Laser-frequency locking to a whispering-gallery-mode cavity by spatial interference of scattered light,” *Opt. Lett.* **41**, 650–652 (2016).
26. W. Zhang, M. J. Martin, C. Benko, *et al.*, “Reduction of residual amplitude modulation to 1×10^{-6} for frequency modulation and laser stabilization,” *Opt. Lett.* **39**, 1980–1983 (2014).
27. B. Sheard, G. Heinzl, and K. Danzmann, “LISA long-arm interferometry: an alternative frequency pre-stabilization system,” *Class. Quantum Gravity* **27**, 084011 (2010).
28. D. Świerad, S. Häfner, S. Vogt, *et al.*, “Ultra-stable clock laser system development towards space applications,” *Sci. Rep.* **6**, 33973 (2016).
29. U. Mishra, V. Li, S. Wald, *et al.*, “Monitoring and active stabilization of laser injection locking using beam ellipticity,” *Opt. Lett.* **48**, 3973–3976 (2023).

30. F. Diorico and O. Hosten, "A robust modulation-free locking of a laser-cavity system," European patent EP 21216871.0 (22 December 2021).
31. F. Diorico and O. Hosten, "A closed loop method and a system for controlling an injection-locked laser," European patent EP 22194904.3 (9 September 2022).
32. A. E. Siegman, *Lasers* (University Science Books, 1986).
33. Y. Aharonov, D. Z. Albert, and L. Vaidman, "How the result of a measurement of a component of the spin of a spin-1/2 particle can turn out to be 100," *Phys. Rev. Lett.* **60**, 1351–1354 (1988).
34. O. Hosten and P. Kwiatt, "Observation of the spin Hall effect of light via weak measurements," *Science* **319**, 787–790 (2008).
35. P. B. Dixon, D. J. Starling, A. N. Jordan, *et al.*, "Ultrasensitive beam deflection measurement via interferometric weak value amplification," *Phys. Rev. Lett.* **102**, 173601 (2009).
36. D. J. Starling, P. B. Dixon, A. N. Jordan, *et al.*, "Precision frequency measurements with interferometric weak values," *Phys. Rev. A* **82**, 063822 (2010).
37. X.-Y. Xu, Y. Kedem, K. Sun, *et al.*, "Phase estimation with weak measurement using a white light source," *Phys. Rev. Lett.* **111**, 033604 (2013).
38. A. N. Jordan, J. Martínez-Rincón, and J. C. Howell, "Technical advantages for weak-value amplification: When less is more," *Phys. Rev. X* **4**, 011031 (2014).
39. J. P. Torres and L. J. Salazar-Serrano, "Weak value amplification: a view from quantum estimation theory that highlights what it is and what isn't," *Sci. Rep.* **6**, 19702 (2016).
40. B. Slagmolen, D. Shaddock, M. Gray, *et al.*, "Frequency stability of spatial mode interference (tilt) locking," *IEEE J. Quantum Electron.* **38**, 1521–1528 (2002).
41. Q.-F. Chen, A. Nevsky, and S. Schiller, "Locking the frequency of lasers to an optical cavity at the 1.6×10^{-17} relative instability level," *Appl. Phys. B* **107**, 679–683 (2012).
42. D. G. Matei, T. Legero, C. Grebing, *et al.*, "A second generation of low thermal noise cryogenic silicon resonators," *J. Phys. Conf. Ser.* **723**, 012031 (2016).
43. L. Jin, "Suppression of residual amplitude modulation of ADP electro-optical modulator in Pound-Drever-Hall laser frequency stabilization," *Opt. Laser Technol.* **136**, 106758 (2021).
44. D. A. Shaddock, B. C. Buchler, W. P. Bowen, *et al.*, "Modulation-free control of a continuous-wave second-harmonic generator," *J. Opt. A* **2**, 400–404 (2000).
45. D. Ottaway, M. Gray, D. Shaddock, *et al.*, "Stabilization of injection-locked lasers using spatial mode interference," *IEEE J. Quantum Electron.* **37**, 653–657 (2001).
46. N. Chhabra, A. R. Wade, E. R. Rees, *et al.*, "High stability laser locking to an optical cavity using tilt locking," *Opt. Lett.* **46**, 3199–3202 (2021).
47. H. Al-Taiy, N. Wenzel, S. Preußler, *et al.*, "Ultra-narrow linewidth, stable and tunable laser source for optical communication systems and spectroscopy," *Opt. Lett.* **39**, 5826–5829 (2014).